Instability of the current sheath implosion in an 18-kJ Mather-type plasma focus

Ming Fang Lu*
Department of Electrical Engineering, Tsinghua University, Beijing 100084, People's Republic of China
(Received 21 December 1995)

An instability phenomenon of the current sheath implosion at the anode (center electrode) end, namely the unstable mode, in a Mather-type plasma focus device (DPF-40, 20 kV, 18 kJ) has been observed. The unstable mode is characterized by rapid slippage of the sliding front of the current sheath along the anode end surface and a ''flat'' sheath configuration caused by an instability phenomenon occurring at the sheath front-anode boundary layer. The unstable mode occurs randomly with respect to a stable mode from shot to shot in consecutive discharges, and significantly influences plasma pinching and neutron yield.
[S1063-651X(96)50207-2]

PACS number(s): 52.55.Ez

The current sheath (CS) implosion at the anode (center electrode) end in a plasma focus, according to the configuration of the magnetic field driving it and the acceleration nature of the CS, is in a macroscopically unstable dynamic equilibrium state. The imploding CS, especially the radial movement of its sliding front, has been found experimentally to be macroscopically stable both in the azimuth and in the (r,z) plane. Also, the typical imploding CS takes an azimuthally symmetric, funnel-shaped configuration with a rather uniform, smooth, and rigid sheath structure, which is considered to be essential for forming a good dense plasma pinch and producing higher neutron yield [1,2]. Specific experimental and theoretical investigations concerning the plasma stability during CS compression in the final implosion phase and immediately prior to pinch formation [3–8] showed that the magnetohydrodynamic (MHD) instability of the imploding CS was avoided either by its acceleration being small enough to satisfy the Kruscal-Shafranov criteria [3–5] or by the stabilization mechanisms of plasma viscosity [4,5] and anomalous plasma resistivity [6,7]. Although such mechanisms may contribute, to some extent, to the stable movement of the CS in the entire implosion phase, investigations directly concerning the stability of the CS implosion have been seldom addressed, possibly because the CS implosion is usually stable, except for some wriggled structures in the CS late in the implosion phase sometimes observed at lower D_2 filling pressures and attributed to the Rayleigh-Taylor (RT) instability [4,9–11]. This problem has not been extensively investigated, and stable implosion of the CS is still not clearly understood. In the present work carried out on a small Mather-type plasma focus device (DPF-40, 20 kV, 18 kJ), we observed, apart from the usually stable imploding CS, an unstable implosion which occurs randomly with respect to the former in consecutive discharges. In this discussion, the former is called the ''stable mode''; the latter, the ''unstable mode.'' They have much influence on plasma pinching and neutron yield. This observation indicates that an instability can develop in the imploding CS, which is contrary to previous understanding. This instability is described in this paper.

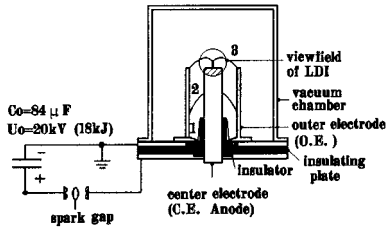

FIG. 1. Schematic diagram of the DPF-40 Mather-type plasma focus device: (1) CS formation in the breakdown phase, (2) CS in the run-down phase and (3) CS in the implosion and pinch phases.

The DPF-40 Mather-type plasma focus device is shown schematically in Fig. 1. It has a coaxial electrode structure with a high aspect ratio. The main parameters of the device are shown in Table I. Deuterium gas with a purity of $>99\%$ was used. The filling pressure varies from 66.5 to 665 Pa, with an optimum pressure of 333 Pa for neutron production. A double-Wollaston-prism laser differential interferometer (LDI) [12] was used to observe the plasma motion, as shown schematically in Fig. 2(a). Since the LDI is intrinsically sensitive to the density gradient, it is suitable in the plasma focus to observe the configuration and structure of the sheath and pinch plasmas by giving direct physical pictures. The light source is a Q-switched yttrium aluminum

TABLE I. Main parameters of the DPF-40 plasma focus device.

Capacitance, C_0	88 μF
Inductance, L_0	79 nH
Charging voltage, V_0	20 kV
Stored energy, E_0	18 kJ
Current rise time, $\tau/4$	$\sim$4 μs
Maximum current, I_{max}	$\sim$350 kA
Center electrode (anode)	diam 64 mm, length 250 mm, copper
Outer electrode	diam 118 mm, 12 stainless steel bars, each 14 mm in diam
Insulator	diam 85 mm, length 35 mm, alumina, with a sharp knife edge groove at the bottom
Filling pressure	66.5–665 Pa, deuterium gas

*Also at Institute of Electrostatics of Hebei University, Baoding 071002, P.R. China, and Institute of Physics of Chinese Academy of Sciences, Beijing 100080, P.R. China. Electronic address: mflu@aphy02.ipy.ac.cn.

TABLE II. Probabilities and neutron yields ($Y_n \times 10^8$ per shot) for the two modes.

Mode	p_{D_2} (Pa)	133	333	532
	Shots	13	25	35
	Probability	56%	52%	(100%)
Stable	Y_n	1.83 ± 0.7	2.1 ± 0.4	0.9 ± 0.6
	Shots	10	23	
	Probability	44%	48%	
Unstable	Y_n	0.9 ± 0.3	0.39 ± 0.2	
	Total shots	23	48	35
Mean	Y_n	1.2 ± 0.6	1.3 ± 0.9	0.9 ± 0.6

garnet laser operated in single-pulse mode. The main parameters of the LDI include an exposure time of about 10 ns, a spatial resolution of about 0.5 mm, and sensitivity about 1.4×10^{25} m^{-4}, which is equivalent to a minimum detectable plasma density of about 1×10^{22} m^{-3} at the plasma-vacuum boundary. A relatively longer exposure time of the LDI limited further quantitative information about the plasmas. The dI/dt signal [Fig. 2(b)] was selected as the time reference for the plasma motion. The spike (S_1) on this signal, corresponding to the collapse of the CS on axis and the beginning of pinching, is set to $t=0$ ns. The times $t<0$ ns and $t>0$ ns correspond to CS implosion and to pinch evolution, respectively. Neutron yield was measured by a calibrated silver activation counter with a relative standard error less than 20% [13].

The anode was a 64-mm-diam solid flat structure with a small radius (transition arc, $R=10$ mm) on the anode edge, as shown in Fig. 3(a). The LDI results of the plasma motion near the anode for 333 Pa are shown in two series of images in Fig. 3. Since the LDI was operated in single-frame mode, the pictures and data in Figs. 3 and 4 for the unstable mode and the stable mode were identified after each group of discharges had been finished, according to the configuration of the imploding current sheath. Each one of the pictures and data was selected from at least four shots. In Fig. 3(b) the CS is just reaching the edge of the anode end and beginning implosion. The images in Figs. 3(c1) to 3(f1) are for discharges which exhibit the instability of the sliding front of the CS at the anode end boundary, while Figs. 3(c2) to 3(f2) are for discharges of the stable mode. From the very beginning of implosion to plasma pinching, the sheath and pinch plasmas show two distinct kinds of configurations and structures. The stable mode of the CS [Figs. 3(c2) to 3(e2)] takes the usually observed azimuthally symmetric, funnel-shaped configuration with a rather smooth, uniform, and rigid sheath structure (the thickness of the sheath is $\delta \sim 1$ mm). Its sliding front is more perpendicular to the anode end surface ($\alpha \sim 68° - 75°$, where α is measured from the anode end surface). For the unstable mode, the CS [Figs. 3(c1) to 3(e1)] shows a rather ''flat'' configuration, with a less perpendicular ($\alpha \sim 16° - 39°$) and more liner sheath structure. Also, the lower part of the CS is thinner ($\delta \sim 0.6$ mm).

TABLE III. Pinch parameters of the two modes for $p_{D_2} = 333$ Pa.

Mode	Length, l (cm)	Radius, $r_{\min}$ (mm)	Duration, τ (ns)
Stable	1.3	1.6	~ 30
Unstable	0.6	1.0	~ 30

Figure 4 gives the axial and radial motion of the two modes of CS, in which v_r represents the radial velocity of the sliding front (also the minimum radial position) and z represents the maximum axial position of the CS measured from the anode end surface. The stable mode always has a higher axial position than the unstable mode ($\Delta z = z_{\text{sta}} - z_{\text{unsta}} \sim 0.3$–$0.6$ cm), but their axial velocities do not show much difference ($v_{z,\text{sta}} \sim 1 \times 10^7$ cm/s and $v_{z,\text{unsta}} \sim 0.9 \times 10^7$ cm/s), as shown in Fig. 4(a). In Fig. 4(b), the implosion of the stable mode is in acceleration, while the unstable mode is in deceleration; especially its sliding front has a large radial velocity in the earlier stage of implosion ($v_{r,\text{unsta}} \sim 2.9 \times 10^7$ cm/s), which is caused by the instability occurring on the sliding front of the CS. This mode is then called the ''unstable mode.'' The instability, according to these observations, is the $m=0$ MHD type but only has a half wavelength and occurs at the plasma-electrode boundary layer. The large radial velocity of the sliding front in the earlier stage of implosion in the unstable mode can be explained as an enhancement due to the smaller impedance,

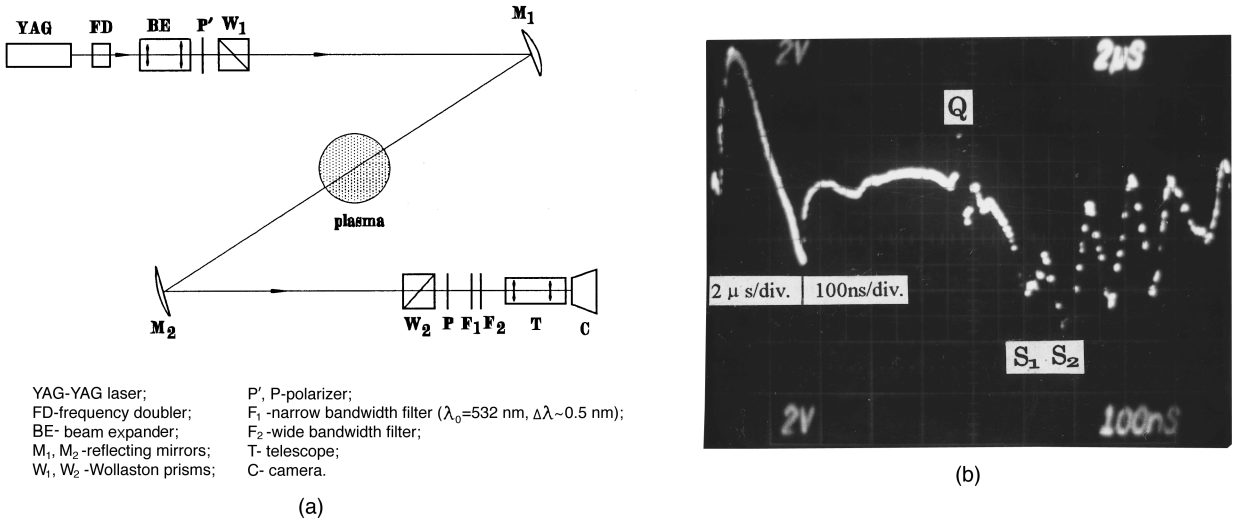

FIG. 2. (a) Optical arrangement of the laser differential interferometry. (b) dI/dt signal for time reference; (Q)- Q-switch signal of the laser (added to the dI/dt signal); (S_1) dI/dt spike by pinch formation, $t=0$ ns.

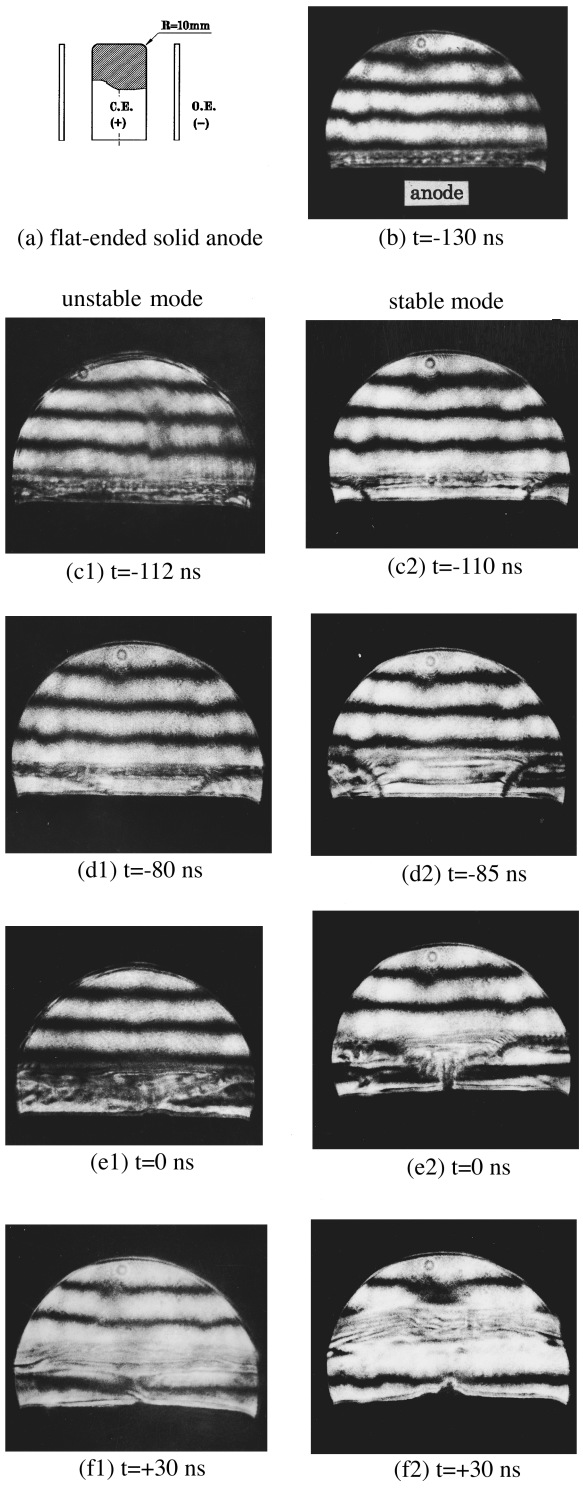

FIG. 3. LDI results of the current sheath implosion and pinch formation; $p_{D_2}=333$ Pa; LDI view field is 60 mm in diameter, side view.

that is, a smaller increase in the space filled with the magnetic field behind the CS, caused by the ''flat'' CS configuration. The increased velocity causes the lower part of the CS to be stretched tangentially and to become nearly a straight line and thinner than the other part of the CS which is less disturbed by the instability ($\delta\sim 1$ mm, and equals that of the stable mode). The overall rigidity of the CS is destroyed. In addition, the imploding CS in the unstable mode is also asymmetric in the azimuthal direction.

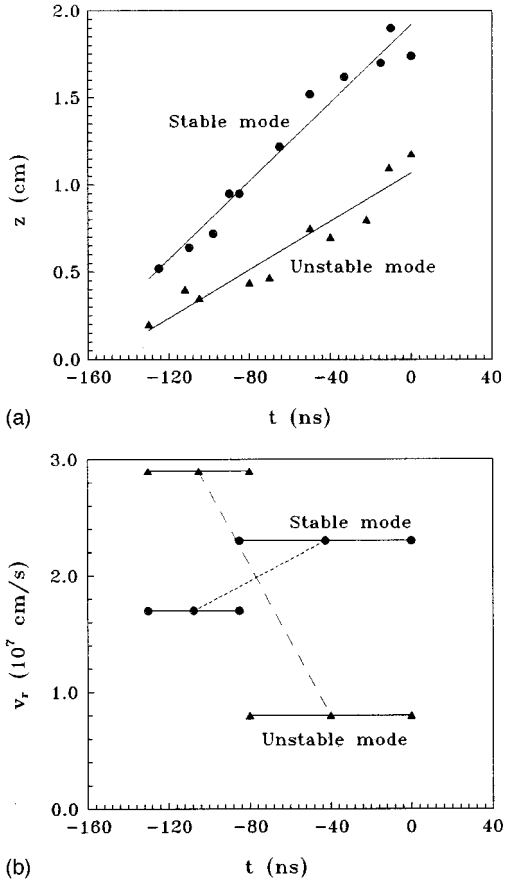

FIG. 4. (a) Axial and (b) radial motion of the current sheaths for the two modes; $p_{D_2}=333$ Pa; in (b), the solid lines represent mean velocities over certain time intervals, and the dashed lines represent deceleration/acceleration trends.

It is found that the unstable mode and the stable mode occur randomly in consecutive discharges with roughly equal probability, as shown in Table II. Neutron yields produced by the two modes at 333 Pa pressure show a systematic difference. The stable mode produces a mean neutron yield about four times higher than that of the unstable mode. The mean neutron yield for a mix of shots is reduced and has large shot-to-shot variation due to the random occurrence of the two modes.

The two modes of the CS form the plasma pinch in different ways. Pinching of the stable mode is partly a result of the gradual radial collapse of the CS on the axis [Fig. 3(e2) and shown schematically in Fig. 5(a)]. The collapsing CS determines the pinching process, and the pinching is not restricted by the CS but advantageous to it. In the unstable mode, axial development of the pinch in the ''flat'' CS configuration tends to lift up the entire CS axially, as shown in Fig. 3(e1) and shown schematically in Fig. 5(b). In this case, pinching is greatly restricted by the CS. Sometimes, the axial

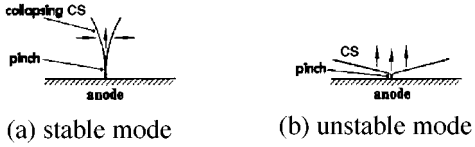

FIG. 5. Schematic of the pinch formation for the two modes: (a) for the stable mode and (b) for the unstable mode.

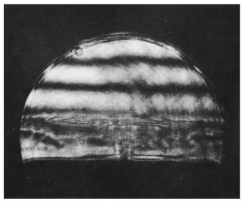

FIG. 6. Current sheath severely distorted by pinching in the unstable mode; $p_{D_2}=333$ Pa; $t=+10$ ns.

development of the pinch causes the CS to be severely distorted and the linear structure of the CS to be destroyed, as shown in Fig. 6. Besides, as the pinch and CS always form a ''T''-type configuration, the stable mode forms a longer pinch and the unstable mode forms a shorter one, as shown in Figs. 3(f1) and 3(f2), and in Table III. The pinching processes of the two modes do not cause systematic differences between their discharge current (I) and dI/dt signals [refer to Fig. 2(b)]. In Fig. 2(b), the spike S_1 and the onset of S_2 on the dI/dt signal correspond to the beginning of the pinching and the cutoff of the pinch by the MHD instabilities at the pinch, respectively. The pinch duration is $\tau\sim 30$ ns, which is nearly the same for the two modes and coincides with the LDI results.

At a lower D_2 filling pressure of 133 Pa, the occurrence of these two modes is similar to that at 333 Pa pressure [see Figs. 7(a) and 7(b) and Table II]. The stable mode still produces a higher neutron yield than the unstable mode; however, the mean neutron yield is less than that at 333 Pa pressure and also has a large shot-to-shot variation. When the pressure is increased to 532 Pa, only the stable mode occurs [Fig. 7(c)]. Under this condition, the CS implodes with a lower radial velocity of $v_r\sim 0.8\times 10^7$ cm/s and the sheath structure is thicker ($\delta\sim 2.3$–3.0 mm). A lower neutron yield results with a large shot-to-shot variation, which is not caused by the instability phenomenon but rather by the pinch dynamics influenced by the higher filling pressure.

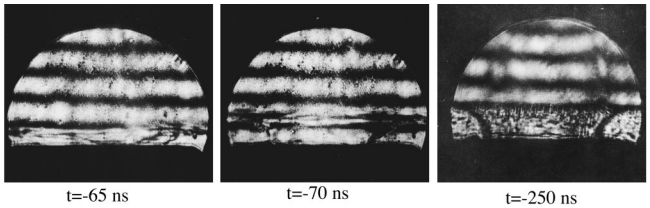

FIG. 7. Current sheath implosion for filling pressures of $p_{D_2}=133$ Pa in (a) and (b) and of $p_{D_2}=532$ Pa in (c).

An instability phenomenon of the current sheath implosion in a Mather-type plasma focus is observed which indicates that the MHD instability in the (r,z) plane can still develop in the imploding current sheath. If the occurrence of the unstable mode is attributed to the unstable dynamic equilibrium state of the imploding current sheath, then the random occurrence of the stable mode under the same operating condition implies the existence of some other stabilization mechanisms to form this mode. This experiment provides a new understanding of the relevant plasma motion, and will help to reveal some unrecognized mechanisms governing this phenomenon. Since the unstable mode negatively influences the plasma pinching and neutron yield, it should be avoided in optimizing the neutron yield from this device, which is consistent with the usual understanding of the relevant plasma motion [1,2].

Further investigations by using series of interrelated anode end structures show that the unstable mode is initiated by the small transition arc ($R=10$ mm) on the anode edge; the random occurrence of the stable mode is due to the stabilization effect on the imploding current sheath by the azimuthal magnetic field introduced in front of the current sheath by an anode end discharge, initiated from the beginning of the main discharge by the ''needle point''-like erosion surface status at the center part of the anode end formed under bombardment by the collapsing pinch plasma. These problems will be described in detail in a future paper.

[1] A. Bernard, *et al.*, Phys. Fluids **18**, 180 (1975).
[2] G. Decker, Physica **82C**, 155 (1976).
[3] N.J. Peacock *et al.*, in *3rd International Conference on Plasma Physics & Controlled Nuclear Fusion Research, Novosibirsk* (IAEA, Vienna, 1968), pp. 51–65.
[4] N.J. Peacock *et al.*, in *4th International Conference on Plasma Physics & Controlled Nuclear Fusion Research, Madison* (IAEA, Vienna, 1971), Vol. I, pp. 537–51.
[5] N.V. Filippov *et al.*, in *4th International Conference on Plasma Physics & Controlled Nuclear Fusion Research* Ref. [4], pp. 573–600.
[6] V.A. Gribkov *et al.*, in *6th European Conference on Controlled Fusion & Plasma Physics, Moscow* (European Physical Society, 1973), pp. 375–8.
[7] V.A. Gribkov *et al.*, Proc. Lebedev Physics Inst. **85**, 193 (1976).
[8] G. Gerdin *et al.*, Plasma Physics and Controlled Fusion **31**, 1341 (1989).
[9] J.P. Baconnet *et al.*, in *9th International Conference on Phenomena in Ionized Gases, Bucharest* (Intrepinderea Poligrafica, Bucharest, 1969), p. 665.
[10] J.P. Rager *et al.*, in *8th International Conference Plasma Physics & Controlled Nuclear Fusion Research* (IAEA Vienna, 1980), pp. 209–21.
[11] M.F. Lu *et al.*, in *1994 International Conference on Plasma Science and Technology 94, Chengdu, China* (Chengdu University of Electronic Science and Technology, Chengdu), p. 150.
[12] W. Merzkirch, *Flow Visualization* (Academic, New York, 1987), p. 135.
[13] M.F. Lu *et al.*, Nucl. Electron. Detection Technol. **14**, 212 (1994).